Propagating high-electric-field domains in semi-insulating GaAs: Experiment and theory

F. Piazza, P. C. M. Christianen, and J. C. Maan
Research Institute for Materials, High Field Magnet Laboratory, University of Nijmegen, Toernooiveld, 6525 ED Nijmegen, The Netherlands
(Received 26 December 1996)

Semi-insulating GaAs exhibits, at a field of about 1 kV/cm, a strong non-Ohmic conduction and negative differential resistance and is consequently suitable for the investigation of nonlinear systems and deterministic chaos. In this paper we explain both experimentally and theoretically, how the homogeneous electric-field distribution loses its stability in favor of a stable, propagating, high-electric-field domain. Furthermore, we provide detailed information about the microscopic structure of the steady-state domain and we explain that the onset of chaos is related to the interaction between subsequent domains. [S0163-1829(97)05324-1]

I. INTRODUCTION

Application of a constant voltage of about 1 kV to semi-insulating (SI) GaAs results in current oscillations caused by the formation of a high-field, high-resistance traveling domain. This experiment is a very simple example of a nonlinear system (here nonlinear resistance) that, for high values of an external control parameter (here the bias voltage), leads to spontaneous symmetry breaking and organizes in coherent structures. For increasing bias voltages these structures become complex and the associated current passes from time independent to periodic oscillations and finally reaches a chaotic behavior. Most experimental work on nonlinear phenomena has been done on hydrodynamics systems or chemical reactions.[1–4] Semiconductor materials in high electric fields have been studied only occasionally in this context, but, despite the excellent material technology and the relative ease of electrical measurements, these studies have not reached the state of maturity of the other systems. The main reason for this state of affairs is that a complete description of the experiment requires the knowledge of the local distribution of current and electric field. They cannot be simply inferred from measurements at the contacts only because the nonlinearity leads to inhomogeneous and time-dependent current and field distributions. In more commonly studied systems such as hydrodynamic instabilities or chemical reactions the analogous local quantities (temperature, pressure, flow, and concentrations) can be made visible more easily.

In a recent paper[5] it has been shown that, by use of an electro-optic technique, it is possible to measure the local, time-dependent field distribution in SI GaAs at high voltages and to show directly domain formation and propagation. In this paper we have employed the same technique, but we have improved the spatial and temporal resolution. Furthermore, with a rigorous theoretical analysis, we explain in detail the formation time and the propagation velocity of the domains and how to relate those experimental quantities to the underlying material parameters. Finally, we show how the transition from Ohmic to periodic and eventually to chaotic behavior takes place. These experiments and their analysis are believed to open the way to a study of chaotic behavior of SI GaAs at high voltages since we can quantitatively define the most relevant underlying properties.

In the following we briefly describe the basic physics of nonlinear transport in semiconductors. In these materials the current density for a spatially homogeneous system is given by the product of the free carrier density n and the carrier drift velocity v_e, which in principle both depend on the electric field E. If the applied voltage is very low, the usual Ohm law applies, with $n=n_0$ and $v_e \propto E$. For larger voltages the dependence of n and v_e on E is more complicated and there may be a region of electric field in which j is decreasing for increasing E ($\partial j/\partial E<0$), i.e., negative differential resistance (NDR). Then the homogeneous charge-density distribution is unstable against a small random density fluctuation and switches to a space- and time-dependent solution. Depending on whether the NDR curve is S or N shaped, the formation of current filaments or traveling high-field domains will take place. If the typical velocity of the domain is comparable to the electron drift velocity the instability is due to a drift nonlinearity ($\partial v_e/\partial E<0$) such as the well-known Gunn domains in n-type GaAs (gigahertz frequencies). On the other hand, slow domain velocities on the order of some cm/s are related to a generation-recombination nonlinearity ($\partial n/\partial E<0$) like in SI GaAs,[6–11] p-Ge,[12] CdSe,[13] and InSb.[14] Even though the specific mechanism depends on the material, in all those cases the dependence of n on E is due to a redistribution of electrons (or holes) between conduction (or valence) band and bound states, which reduces the number of free carriers. The detailed local measurement of the electric field presented here for SI GaAs will allow the determination of this redistribution of charge.

The rest of this paper is organized as follows. In Sec. II we present the experimental details including a description of the electronic structure of GaAs and in Sec. III the experimental results regarding the relation between electric field and current, the domain formation, and the domain steady-state propagation. Finally, in Sec. IV we analyze the structure of a propagating steady-state domain to obtain the free and trapped carrier distributions, the trapping coefficient dependence on the electric field, and the relation between domain velocity and material parameters.

II. EXPERIMENT

The experimental setup is similar to that described in Ref. 5 and is briefly outlined below. The experiment is based on

the longitudinal electro-optic effect of a $Bi_{12}SiO_{20}$ (BSO) crystal to transform a voltage distribution in a phase shift of light (Fig. 1). The crystal has a transparent electrode (indium tin oxide) on the front and a dielectric mirror (maximum reflectivity of 99.8% at 780 nm) on the back and it is put with the back side on top of the sample. An expanded polarized laser beam from a 780-nm diode laser enters the crystal through the transparent electrode and is reflected back by the mirror through a beam splitter and an analyzer. Grounding the top electrode of the BSO, the phase shift induced by the voltage difference between the two sides of the crystal, which corresponds to the voltage distribution on the sample, is recorded as a light intensity distribution on a charge coupled device camera and is digitized with a frame grabber. The relation between voltage and light is determined through an *in situ* calibration and thus does not rely on any material parameters, providing a resolution of the system of 10 V. A homemade electronic controller allows us to synchronize the laser source and the readout of the camera with the current oscillations and to control the number of active lines in the camera. Decreasing the number of active lines reduces the amount of redundant information and increases the time resolution of the system up to 100 kHz.

Liquid encapsulated Czochralski (LEC) GaAs is used since it is a suitable semiconducting material for our investigation because its high resistivity implies high applied voltages and the current oscillations have low frequency. Both facts make the detection of the time-dependent voltage profile easier. The high resistivity is caused by the trapping of conduction-band electrons in the EL2 midgap donors,[15] which compensate the residual shallow donor (concentration N_D) and acceptor (concentration N_A) charges.[16] EL2 defects are double donors, which are neutral when occupied by an electron and singly or doubly charged when ionized. The doubly ionized level is not relevant for the compensation. Therefore, at room temperature the Fermi level is pinned at the energy of the EL2 traps, which are partially ionized and in equilibrium with electrons in the conduction band via trapping (coefficient C_n) and emission (rate X_n). Both shallow donors and acceptors are fully ionized and they are relevant only as charge background. The trapping coefficient is strongly enhanced by the electric field,[15,4] leading to the depletion of the free electrons in the conduction band and to a growing number of trapped electrons in the EL2 levels (n_{EL2}). Thus, with increasing electric field the number of carriers is reduced, increasing the resistivity and causing N-shaped NDR.[18,19] One model explains the field-enhanced trapping in terms of a configurational barrier of 60 meV due to a multiphonon capture process that requires an electric field of about 0.5 kV/cm to be overcome.[15] The other model proposes an enhanced capture of hot electrons in the L valley that occurs at about 3.0 kV/cm.[20] In any case, the NDR in SI GaAs is a well established phenomenon and is responsible for the slow domains studied in this paper.

We have used three samples, obtained from two different ⟨100⟩ LEC-grown single-crystal GaAs wafers with different contact characteristics. Sample (a) has been obtained from a slab with mobility $\mu = 0.66\ \mathrm{m^2/V\,s}$ and resistivity $\rho = 3.1 \times 10^7\ \Omega$ cm, with a thickness of 0.5 mm. Two linear Au contacts have been evaporated 8 mm apart without any annealing. Samples (b) and (c) came from a slab with $\mu = 0.63\ \mathrm{m^2/V\,s}$ and $\rho = 7.0 \times 10^7\ \Omega$ cm and we have provided them with two NiAuGe contacts 8 mm apart for sample (b) and 6 mm apart for sample (c) and annealed for 10 min at 430 °C.

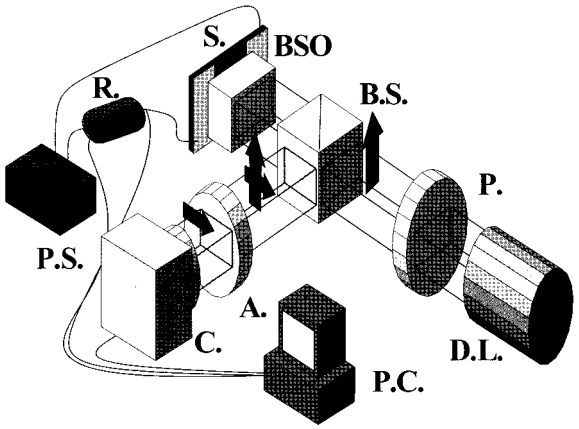

FIG. 1. Experimental setup. The arrows indicate the light polarization that changes as a function of the voltage on the surface of the sample. The symbols have the following meaning: DL, diode laser; *P*, polarizer; BS, beam splitter; BSO, electro-optic crystal; *S*, sample; *A*, analyzer; *C*, camera; *R*, resistor; PS, power supply; PC, personal computer. The front of the BSO is covered with a indium-tin-oxide layer used as a transparent electrode and the back with a dielectric mirror.

III. RESULTS

The experiment has been performed on all the three samples, which showed the same qualitative behavior. Therefore, only the results obtained for sample (a) are shown.

The current as a function of the bias voltages (Fig. 2) exhibits three characteristic regions: time independent for voltages below V_{c1}, periodic oscillations for $V_{c1} < V < V_{c3}$, and chaotic in time for $V_{c3} < V$. Figure 2 shows the peak and valley value of the current signal as a function of the applied voltage and, in the periodic region, the value of the fundamental frequency. For $V < V_{c1}$ the current is proportional to the voltage and thus the behavior is Ohmic, with the same resistivity as the original slab. The electric-field distribution is homogeneous, except for a small region near the contacts, where the depletion layer enhances the resistivity.[5] The periodic region can be further subdivided in two parts ($V_{c1} < V < V_{c2}$ and $V_{c2} < V < V_{c3}$) separated by a drop in the current fundamental frequency at V_{c2}. In both parts the frequency is growing superlinearly, from almost 0 to 15 Hz in the first one and from 4 to 12 Hz in the second one. The frequency drop corresponds to a qualitative change of the current signal. In the low-voltage part it consists of a single spike over a constant background signal (Fig. 3, curve *a*), while in the high-voltage part, two different spikes are repeated periodically (Fig. 3, curve *b*). When V_{c3} is exceeded, the current signal remains time dependent, but with an erratic behavior, which makes it impossible to define a fundamental frequency[21–23] (Fig. 3, curve *c*).

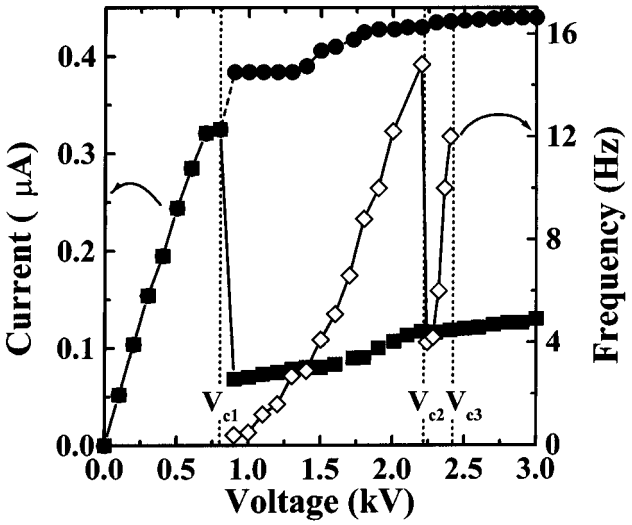

FIG. 2. Current signal as a function of the bias voltage. The continuous-line with squares is the minimum and the dotted line with circles is the maximum of the current. For $V<V_{c1}$ the sample behaves Ohmically, for $V_{c1}<V<V_{c3}$ periodic spikes in the current appear, and for $V>V_{c3}$ the current is still oscillating, but not periodically. In the periodic regime, the oscillation frequency has been plotted (diamonds).

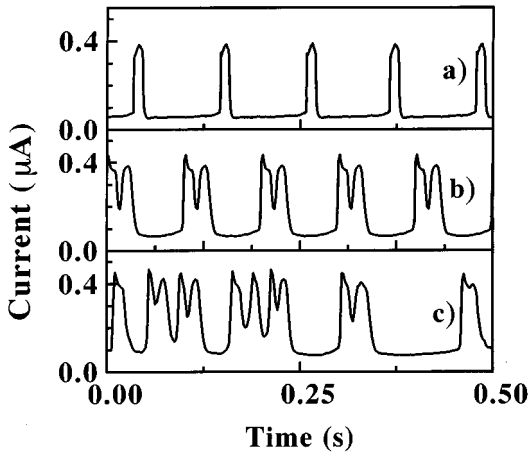

FIG. 3. Current signal as a function of time. The applied voltage is 2.00 kV for curve *a*, 2.35 kV for curve *b*, and 2.80 kV for curve *c*.

A. Periodic propagation

For applied voltages $V_{c1}<V<V_{c2}$ (Fig. 4), when the current is low, a high-electric-field domain is propagating from the anode, where it is formed, to the cathode, where it dis-

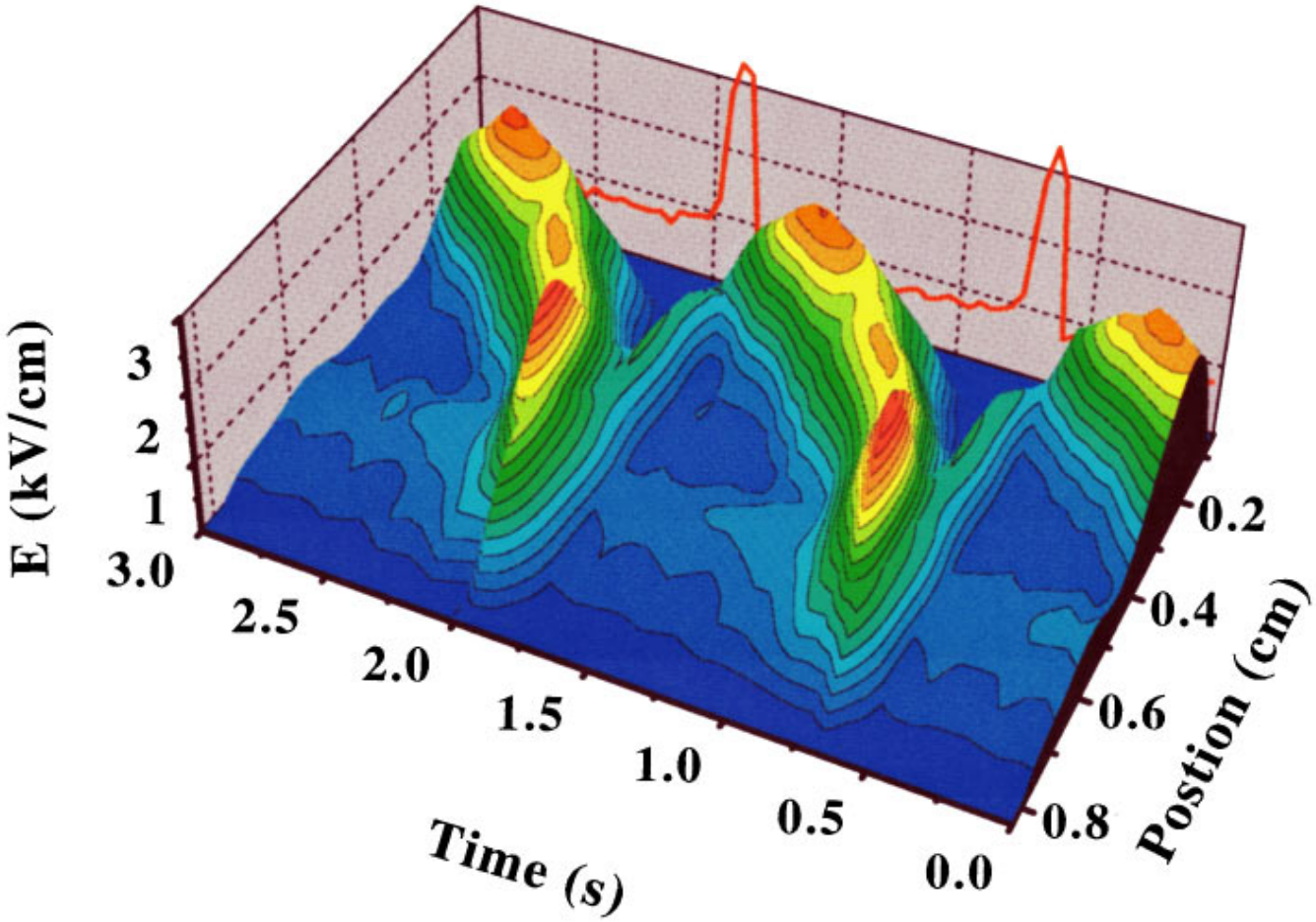

FIG. 4. (Color) Electric-field profile of a domain propagating in the sample as a function of position and time (3D plot) and current signal as a function of time (continuous line). The anode is at $x=0.0$ cm and the cathode is at $x=0.8$ cm. The spike in the current corresponds to a constant electric-field distribution. The measurement has been performed on sample (a) biased with $V=1.0$ kV.

appears. The domain remains parallel to the contact and the voltage profile does not depend on the distance from the edge. Thus, for a complete description, it is sufficient to plot the electric field, obtained by differentiating the voltage profile, as a function of the distance from the anode (Fig. 4). The domain is propagating with an approximately Gaussian shape and the periodic spikes in the current signal correspond to an almost homogeneous field during the process of annihilation of one domain and the creation of the next one.

The domain does not travel across the entire sample with constant velocity and shape, as often stated in literature. Instead it reaches a steady-state configuration only after a transient time and length in which it grows and simultaneously slows down. We describe the electric-field peak position as a function of time (Fig. 5) with the function $x_{\text{peak}}=\tau_f(v_0-v_d)[1-\exp(-t/\tau_f)]+v_d t$, where τ_f is the domain formation time, v_0 is the domain initial velocity, and v_d is the steady-state domain velocity. The quality of the fit to the data and the values of the fit parameters are shown in Fig. 6 for different applied voltages.

The drastic change in the sample behavior around V_{c1} corresponds to a bifurcation in which the spatially homogeneous solution loses its stability while a new stable solution, with lower symmetry, emerges.[2] For applied voltages larger than V_{c1} a homogeneous electric field is in principle still allowed, but every fluctuation is amplified and the system is driven to the stable configuration corresponding to a steady-state domain propagating with constant velocity.[1,18] The propagating domain is completely stable only in an ideal infinite sample, while in our case it has to be annihilated at the cathode. During this process, the electric field outside the domain grows to maintain the voltage drop over the sample constant. Since the homogeneous solution is unstable and for a short time a homogeneous electric field $E=V/d$ exists in the sample, the domain formation at the anode corresponds to the relaxation of the unstable homogeneous electric-field distribution toward a stable steady-state propagating domain. The experimental data in Fig. 5, which describe the transition from the homogeneous electric field to the propagating domain, are properly interpolated by the fitting curve. It is surprising that a simple exponential is sufficient to describe the complete transition because it is expected to hold as linear approximation only nearby a steady state. The formation time τ_f (Fig. 6) is about 12 ms and does not depend on the applied voltage, suggesting that it is related to material parameters.

The steady-state domain simply propagates, preserving its shape, and it is completely described by its electric-field profile as a function of the position (Fig. 7, top) and its constant velocity (Fig. 6). The velocity is found to depend linearly on the applied voltage. In the literature the domain velocity is usually systematically overestimated because it is obtained directly from the current pulse frequency under the assumption of constant propagation velocity, which is not true because during its formation the domain moves faster, as shown here. In Fig. 8 we present the electric-field peak and the domain half-width at half maximum (l_d) as a function of the applied voltage. The domain width is about 0.1 cm for all the studied voltages, while the height grows proportionally with the applied voltage from 3 to 8 kV/cm. The shape of the domain remains in a good approximation Gaussian for every applied voltage, in contrast with Gunn domains, which, for high voltages, are flat topped.

B. Aperiodic propagation

For bias voltages $V_{c2}<V<V_{c3}$ the periodicity is no longer due to the repetition of domains with the same dimension, but to two alternating domains with different dimensions [Fig. 9(a)]. The arrival of a domain corresponds to a current spike and thus a single period in the current signal consists of two different peaks (Fig. 3, curve *b*). The bifurcation in the electric-field pattern does not correspond to a current frequency doubling because of the complex relation between the domain velocity (and thus the current frequency) and the domain dimension. If the voltage is increased further, the current is clearly aperiodic and no evidence is found for subsequent bifurcation indicative for routes to chaos. The observed distribution of electric fields shows that domains with different sizes appear consecutively, but that at each moment only one domain is present in the sample. This can be seen in Fig. 9(b), where, at every time, the electric-field distribution has only one maximum, which defines the domain position. The reason why the current oscillations become aperiodic can be inferred from Fig. 5, which shows that the extension of the transient length for increasing voltages becomes comparable to the extension of the sample length for $V=V_{c2}$. Thus, for $V>V_{c2}$, the domains are not able to reach a steady-state configuration and are still growing while they reach the cathode. Therefore, the growth of one domain is influenced by the annihilation of the previous one and the two domains' sizes are strongly correlated. This process leads to chaotic oscillations in the current through the recursive interaction between successive domains during the annihilation-creation process. The impossibility to see more than one bifurcation in the electric-field pattern is probably due to the relatively high level of noise intrinsic in high resistance samples.

From data in Fig. 5 it is interesting to predict, for different samples, at which applied voltages the oscillations are periodic or chaotic once the sample length L is known. In sample (a) the quantity $E_c=(V_{c3}-V_{c1})/L$ is 2.0 kV/cm, but this cannot be directly generalized because of the complex behavior of $x_{\text{peak}}(t)$. To fix an upper and a lower limit for E_c, independently of the sample length, we calculate the distance the domain takes to form completely, supposing it moves with constant velocity for a time τ_f. As already discussed, the velocity of a forming domain is not constant but is monotonical decreasing from the starting one v_0 to the final one v_d. The upper limit in E_c is then obtained using v_d and the lower limit using v_0. The possibility to normalize the applied voltage over the sample length comes from the fact that also v_0, and not only v_d (Fig. 6), is proportional to $V_{c3}-V_{c1}$. Once the two proportionality factors are known, we calculate the two E_c values, which are 0.7 and 26 kV/cm. The actual value for our sample is closer to the lower limit because v_0 is one order of magnitude larger than v_d and then it is dominant in fixing the formation length.

IV. DISCUSSION

The basic equations for nonlinear electronic transport in the presence of generation and recombination dynamics are

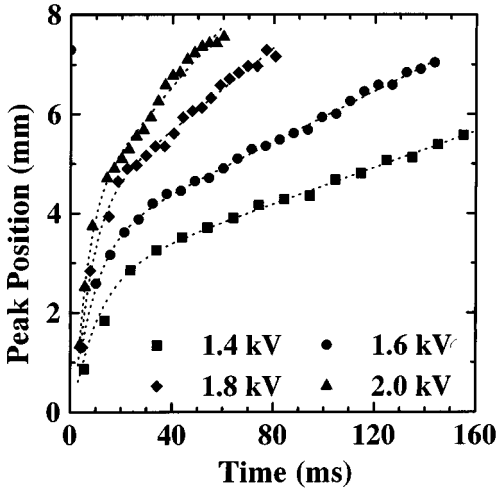

FIG. 5. Electric-field peak position as a function of time for different applied voltages. The dotted lines are the results of the fits described in the text.

the Poisson equation, the current continuity, the current equation in the drift-diffusion approximation, and the rate equation for n_{EL2},[1]

$$\frac{\partial E}{\partial x}=\frac{q}{\varepsilon\varepsilon_0}\rho, \tag{1}$$

$$\frac{\partial j}{\partial x}=\frac{\partial \rho}{\partial t}, \tag{2}$$

$$j=q\left(n\mu E+D\frac{\partial n}{\partial x}\right), \tag{3}$$

$$\frac{\partial n_{\mathrm{EL2}}}{\partial t}=C_n(E)(N_{\mathrm{EL2}}-n_{\mathrm{EL2}})n-X_n n_{\mathrm{EL2}}, \tag{4}$$

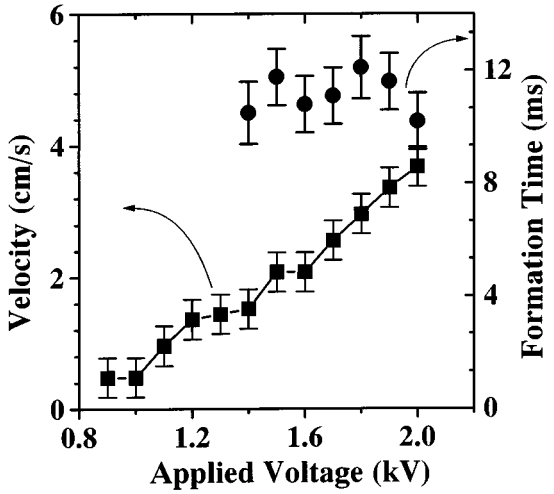

FIG. 6. Domain velocities (squares) and formation times (circles) for different applied voltages obtained from the fits of Fig. 5.

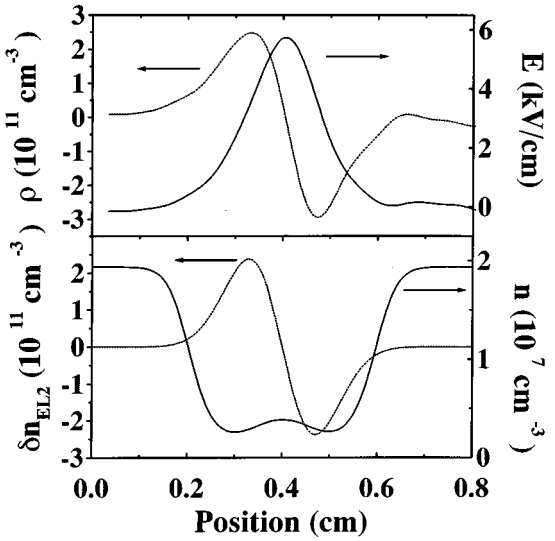

FIG. 7. Top: measured electric field (solid curve) and charge distribution (dashed curve) as a function of the position for an applied voltage of 1.4 kV in sample (a). Bottom: evaluation of the conduction-band electron density n (solid curve) and the density fluctuation δn_{EL2} (dashed curve) of the EL2 trapped electrons from the data on top.

where q is the electron charge, ε_0 and ε are the dielectric constants of vacuum and GaAs, μ is the electron mobility, D is the electron diffusion coefficient, and ρ is the charge density in the number of electron charges. In general, j, ρ, n, and n_{EL2} may depend on x, t, and E, while μ, D, C_n, and X_n may depend on E. Equations (1)–(3) are very general and can be applied to describe transport in every semiconductor. Equation (4) describes trapping and thermal emission processes, which are the most relevant generation-recombination processes in our system. The material parameters used in the calculation are presented in Table I. Although these equations are standard, their solution is very complicated because of the x and t dependence of most of the variables. This complication reflects the unusual regime

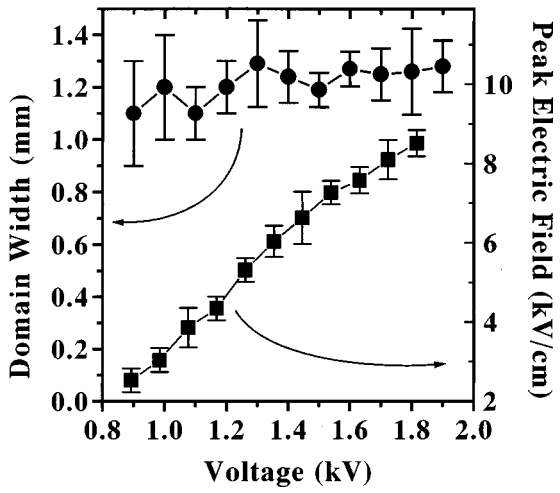

FIG. 8. Electric-field peak value (squares) and half-width at half maximum (circles) of the domain as a function of the applied voltage in sample (a).

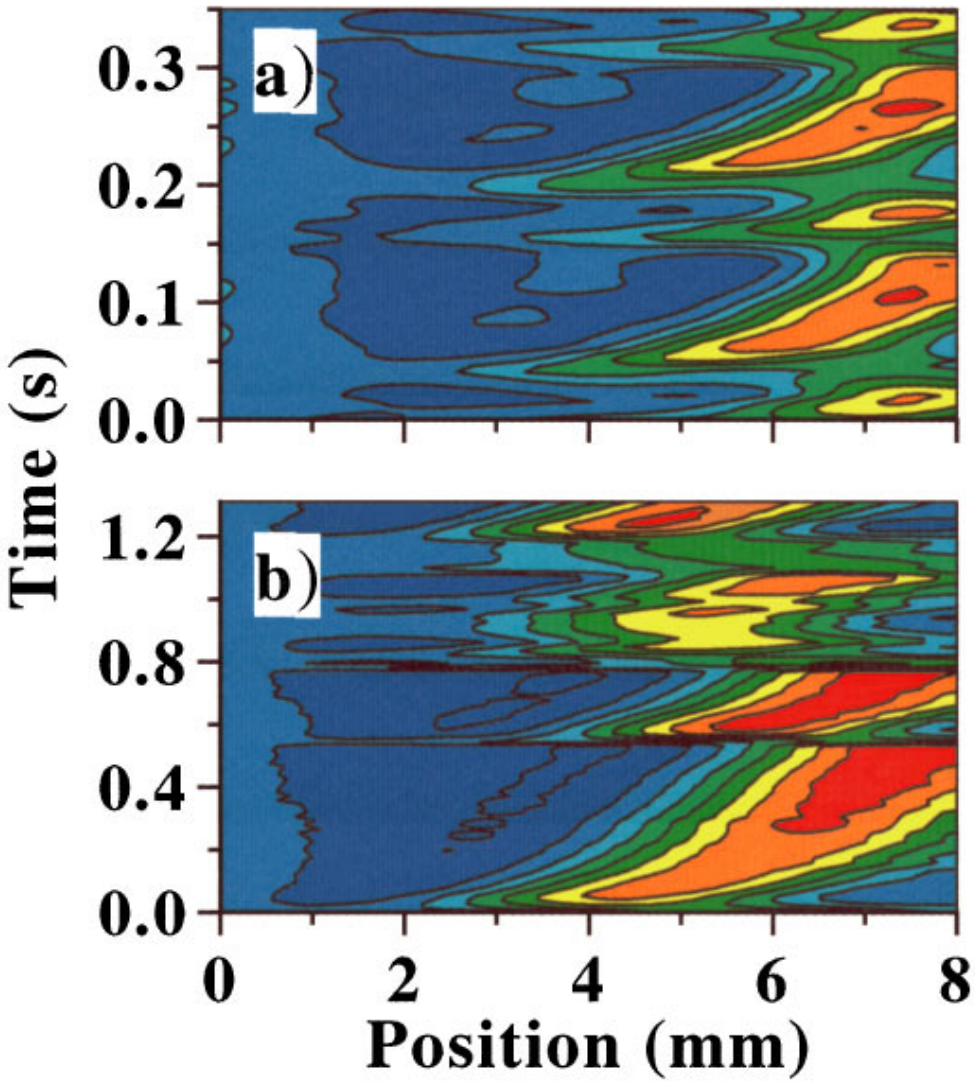

FIG. 9. (Color) Measured electric-field distribution as a function of position and time. The color scale extends linearly from 0 kV/cm (blue) to 9 kV/cm (red). The applied voltage is (a) 2.3 kV and (b) 2.6 kV.

for electrical conductivity. In normal metals the high carrier density leads to a very short screening length and to a very fast relaxation of any charge fluctuation, which always leads to local charge neutrality. In semiconductors this is not always the case and we are familiar with space-charge effects through differences in the chemical potential (either through doping or through external electric field). However, here we are confronted with a nonequilibrium process, and normal concepts, for instance, chemical potentials, are not applicable. Furthermore, the very low carrier density leads to wide space-charge regions (of the order of some millimeters) and to very slow relaxation of charge fluctuations (relaxation regime). These unique conditions of electrical transport have been poorly studied, but they are at the basis of the understanding of nonlinear electrical transport. The very detailed experimental data described above provide a solid basis for studying Eqs. (1)–(4) in detail in any conditions.

TABLE I. Material parameters used in the model. The values of N_A and N_D are obtained by the substrate supplier by glow discharge mass spectroscopy.

Quantity	Value	Source
n^0	1.9×10^{7} cm^{-3}	measured
N_A	2.2×10^{15} cm^{-3}	measured
N_D	1.3×10^{15} cm^{-3}	measured
N_{EL2}	1.3×10^{16} cm^{-3}	Ref. 16
n^0_{EL2}	0.9×10^{15} cm-3	Ref. 16
$C_n(0)$	2.0×10^{-8} cm^3/s	Ref. 17
X_n	5.7×10^{-2} s^{-1}	Ref. 17

A. Domain formation

In Eqs. (1)–(4), E, ρ, j, n, and n_{EL2} are related variables, while $\mu(E)$, $D(E)$, $C_n(E)$, and $X_n(E)$ are material constants. $\mu(E)$ is very well established theoretically and experimentally.[24] We have used a mobility $\mu(E)$ as given for ultrapure GaAs, which is a good approximation for our sample because at room temperature the mobility is limited by an electron-phonon interaction.[25] The diffusion coefficient D is obtained directly from μ using the Einstein relation. $C_n(E)$ and $X_n(E)$ have been calculated as reported in

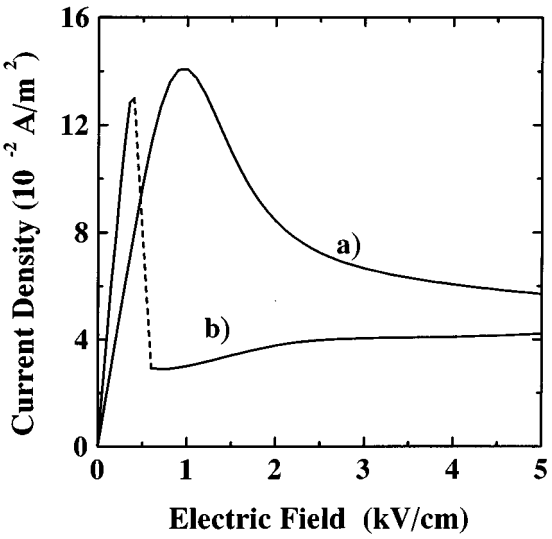

FIG. 10. Current density as a function of the electric field obtained from the homogeneous solution of Eqs. (1)–(3). For curve *a* we have used the values of C_n reported in Ref. 1, while for curve *b* we have used experimental values.

Ref. 1. Although all material parameters are known, still, from a mathematical point of view, an infinite number of possible solutions of these equations exist, depending on the initial conditions. Therefore, the question is to determine the solutions that are stable and thus physically relevant.

The most simple is the homogeneous one, which is obtained by setting all the derivatives in time and space equal to zero. Then there is no space-charge accumulation anywhere (local charge neutrality) and there is no time dependence in the solutions (steady state). Equations (1)–(4) reduce to Eqs. (3) and (4) only, which describe Ohm's law [Eq. (3)] and a balance equation for the carrier density [Eq. (4)]. In this regime we can calculate $j-E$ (Fig. 10, curve *a*) using the values of $C_n(E)$ and $X_n(E)$ presented in Ref. 1. For electric fields below 1 kV/cm, the system behaves Ohmically and the calculated curve $j-E$ reproduces the data presented in Fig. 2. When the electric field exceeds a certain critical electric field, we enter a region where, in principle, the homogeneous solution is still present but it is unstable. It can be shown that in a system with positive differential resistance, all the charge fluctuations decay with increasing length or time and the system will therefore return to the homogeneous solution. In systems with NDR, every charge or electric-field fluctuation is amplified in time or space. The characteristic time with which charge fluctuations will grow depends on the $j-E$ curve and is given by $\tau_d = (dj/dE)(1/\varepsilon\varepsilon_0)$,[8,25] which is negative, indicating that inhomogeneities are amplified, instead of damped as in the Ohmic case. Assuming that the curve in Fig. 10 can also be used to describe when the domain is forming, τ_d is about 5 ms. This number is quite close to the formation time of 12 ms experimentally observed. The process of domain formation may be explained in the following way. There will always be charge fluctuations near the contact. These fluctuations are amplified above V_{c1}, leading to a growing domain, starting from the contact, with a characteristic time τ_f. Experimentally, we observe that this growth stops once the domain has reached a critical size and amplitude. Once this has occurred, the stable domain propagates with constant shape and velocity.

B. Steady-state domain

1. Free and trapped electron distributions

In the previous calculations, $C_n(E)$ and $X_n(E)$ are estimated theoretically and then used in the model to explain the experimental results. The quantitative measurement of the electric-field profile allows a different approach, in which we evaluate the unknown quantities, including $C_n(E)$, using the experimental electric-field distribution as the solution of the set of equations.[26] The steady-state domain apparently is a physically acceptable solution of Eqs. (1)–(4). As observed, this solution allows a time and position dependence of $\rho(x,t)$, $n(x,t)$, and n_{EL2}, which is neither constant (as discussed above for the Ohmic solution) nor growing or decaying with time and position. We can analyze this particular solution by transforming in Eqs. (1)–(4) $f(x,t) \rightarrow f(x-v_d t)=f(x')$. Integrating Eq. (2) between a generic position and a point far from the domain and combining it with Eq. (3) results in

$$J_0-\rho(x')v_d=n(x')\mu E(x')+D\,\frac{\partial n(x')}{\partial x'}, \tag{5}$$

where J_0 is the current density measured at the contacts far from the domain, which has a constant value as a result of the boundary conditions coming from the integral. The sum of the drift current, the diffusive current, and the displacement current due to the movement of the charge dipole connected to the domain (ρv_d) is constant all over the sample. This is consistent with the fact that there is no space-charge accumulation when the domain is in the steady state since the shape remains the same. The current J_0 and the electric-field profile $E(x)$ are experimentally obtained, while $\rho(x)$ can be directly evaluated from experimental data using Eq. (1) (typical results are shown in Fig. 7). $n(x)$ can then be calculated from Eq. (5) since it is the remaining undetermined quantity, and the results are shown at the bottom of Fig. 7. It is interesting that the maximum value of the dipole charge ρ is four orders of magnitude larger than n_0, the equilibrium concentration of electrons in the conduction band, showing directly that the positive side of the dipole cannot be obtained considering only free electrons.

From the data it becomes clear that the contribution to the current is almost completely due to the drift of the electrons in the conduction band because the term $n\mu E$ is about four orders of magnitude larger than ρv_d and eight larger than $D(\partial n/\partial x')$. This makes the properties of slow domains very different from that of Gunn domains, where the displacement current is more relevant. Then, considering only the most relevant term in Eq. (5), we find that

$$n(x')\approx\frac{J_0}{\mu E}. \tag{6}$$

Since J_0 is a constant, while in the domain region E increases, Eq. (6) shows that the major effect of the high field on the conduction-band electrons is a decrease in density of almost 80% (Fig. 7). Once $n(x)$ is known, we can evaluate

the number of trapped electrons as $n_{EL2}(x)=N_{EL2}-n(x)-\rho(x)-N_A+N_D$. From this result we can plot (Fig. 7) the variation of trapped electrons as $\delta n_{EL2}=n_{EL2}-n^0_{EL2}$, where the last term is the zero-field value. This variation is quite small compared to the total number of trapped electrons; therefore, n_{EL2} itself hardly varies over the sample since the maximum value of ρ is only 0.1% of n^0_{EL2}. Figure 7 directly shows the relation between ρ and δn_{EL2} and thus demonstrates that the domain charge dipole originates from a fluctuation of trapped electrons around the equilibrium value. Considering that the trapping and ionization times for electrons depend on the number of trapped electrons [Eq. (4)], we can explain the symmetry of the domain by the fact that $\delta n_{EL2} \ll n^0_{EL2}$ and thus that generation-recombination dynamics are, in a first approximation, roughly the same on the right- and on the left-hand side of the domain. Strictly speaking, Eq. (6) relates the current outside the domain to n, μ, and E in the domain and thus to the local value of the current. It is, however, reasonable, as explained before, to assume that a constant current J_0 is actually flowing through the whole domain region. Neglecting the displacement current, this fact implies that the continuity equation (3) is automatically fulfilled and that the high-field conductivity $\sigma(E)$ must be inversely proportional to E. It follows directly from the previous analysis that this particular $\sigma(E)$ dependence directly leads to a domain propagating with constant velocity.

2. Trapping coefficient

Once the number of electrons in the conduction band and in the EL2 levels is known locally and for a large range of electric fields, we evaluated the dependence of $C_n(E)$ on E. The equations have been simplified considering that the time scale of the perturbation on n and n_{EL2} caused by the moving domain is 0.1 s (l_d/v_d), while the dominant relaxation time in Eq. (4) is 10^{-9} s ($C_n N_{EL2}$), showing that the time derivative in Eq. (4) can be neglected. Thus the free and trapped electrons are, for every value of the electric field, in local equilibrium and the ratio between them is completely decided by the value of the trapping coefficient determined by the local electric field. This statement does not mean that the system is globally in thermal equilibrium but it implies that the energy distribution of the electrons in the conduction band is described locally by the field-dependent trapping and emission coefficients. The trapping coefficient can be directly evaluated from Eq. (4):

$$C_n=\frac{X n_{EL2}}{(N^0_{EL2}-n^0_{EL2})n}, \tag{7}$$

in which the only quantity that is relevantly changing with the field is n, showing an enhancement of C_n in the high-electric-field region, where n is depleted (Fig. 11). The emission rate X_n is considered constant for electric fields up to 100 kV/cm.[27] C_n has been evaluated from data obtained for seven different applied voltages and a unique curve is obtained, although the peak electric field and the domain velocity vary by at least a factor of 2, proving the consistency of our analysis.

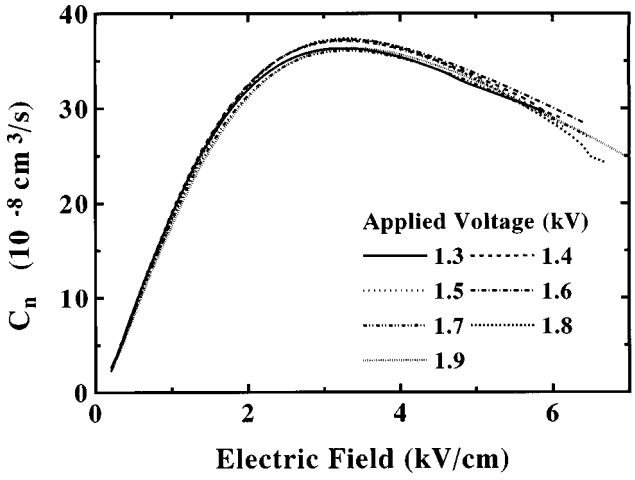

FIG. 11. Electron trapping coefficient C_n in EL2 levels as a function of the electric field obtained for domains at seven different applied voltages.

The trapping rate is seen to increase almost linearly by a factor of 15, for electric fields on the order of 3 kV/cm, where it reaches a maximum after which it slowly decreases. The plot shows that the trapping enhancement already starts at electric fields much lower than those needed for intervalley scattering, indicating that the electrons have to overcome a much smaller barrier. Thus the mechanism of a configurational barrier due to multiphonon trapping, which is found to require an electric field of only 0.5 kV/cm for the onset of electron capture, is fully consistent with our experimental results.[26]

Once C_n is known from the experiment over the whole field range, we have used again Eqs. (1)–(4) to evaluate the $j-E$ relation for the homogeneous electric-field distribution (Fig. 10, curve b). The C_n values plotted in Fig. 11 cannot be extrapolated to electric fields lower than 0.4 kV/cm, which is the minimum measured value when a domain is present in the sample. Therefore, the low-field values are obtained measuring locally the electric field in the contact region where the transport is Ohmic. The most relevant differences between curves a and b regard the critical electric field, which in our case is about 0.4 kV/cm instead of 0.8 kV/cm, and the behavior of j for large E values, which in our case is increasing instead of decreasing.

3. Domain velocity

The previous discussion, based on Eq. (6), which is a first-order approximation of Eq. (5), does not explain the velocity of the domain and the origin of the fluctuation of trapped carriers δn_{EL2}. Moreover, it appears strange that a symmetric electric-field distribution E and a symmetric free-electron distribution n correspond to an antisymmetric trapped electron distribution (Fig. 7). To explain this inconsistency we improved the approximation of Eq. (6) including the next relevant term of Eq. (5), which is the displacement current $v_d\rho$, leading to the equation of the free electrons

$$n(x)\simeq\frac{J_0}{\mu E}-\frac{v_d\rho}{\mu E}=\frac{J_0}{\mu E}-\delta n, \tag{8}$$

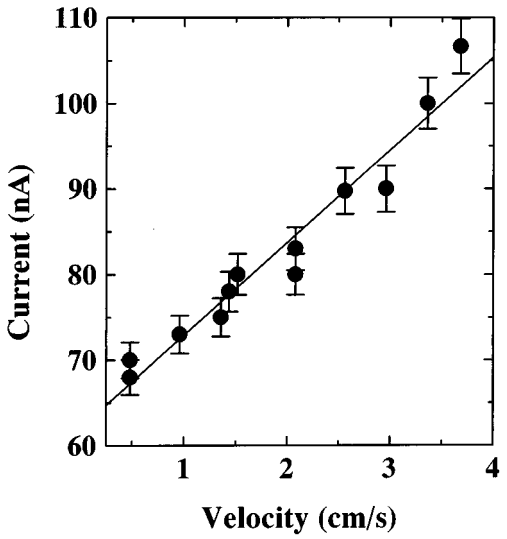

FIG. 12. Constant minimum in the current (circles) as a function of the domain velocity measured in sample (a). Every point corresponds to a different applied voltage. The linear fit of the data is plotted with a continuous line.

where $\delta n = v_d \rho / \mu E$ is treated as a small perturbation. δn cannot be attributed to a variation of the trapping coefficient because, for the same value of E on the right- and on the left-hand side of the domain, the two corresponding values of ρ have an opposite sign and thus it has to be attributed to the formation of space charge in the n distribution. The fluctuation in n is by far too small to form directly the whole charge dipole ρ, but, through the generation-recombination process of the EL2 levels, give rise to a fluctuation δn_{EL2} around n^0_{EL2}. Considering Eq. (4) we can see that

$$\frac{\delta n}{n} \simeq \delta n_{\mathrm{EL2}} \left(\frac{1}{N_{\mathrm{EL2}} - n^0_{\mathrm{EL2}}} + \frac{1}{n^0_{\mathrm{EL2}}} \right). \tag{9}$$

It is interesting to notice that because of the large value of n_{EL2} with respect to n $(n/n_{\mathrm{EL2}} \simeq 10^{-8})$, the displacement current due to the domain movement is the ultimate origin of the large charge dipole that is necessary to sustain the domain itself. Thus the generation-recombination process between two very different populations amplifies the effect of the displacement current. Moreover, a domain that reaches the cathode and is forced to stop will disappear because no displacement current is present anymore. On the other hand, a domain that is moving with a velocity larger than the steady-state velocity, like during the formation, will grow. Therefore, the only possible nonhomogeneous steady-state solution is a domain traveling with constant velocity. Substituting Eq. (6) into Eq. (9), we find that

$$v_d \simeq \frac{J_0}{n^{\mathrm{eff}}_{\mathrm{EL2}}}, \tag{10}$$

where

$$n^{\mathrm{eff}}_{\mathrm{EL2}} = \frac{1}{N_{\mathrm{EL2}} - n^0_{\mathrm{EL2}}} + \frac{1}{n^0_{\mathrm{EL2}}} \tag{11}$$

is the weighted balance between free and occupied states in the EL2 traps. A similar relation between domain velocity and current signal has been proposed by Sacks and Milnes[7] and Ridley and co-workers[8] on an empirical basis and has been experimentally confirmed,[7,28–30] but up to now no explanation had been proposed. In Fig. 12 we show that the relation between J_0 and v_d measured for different bias voltages is indeed linear. From the slope, a value of $n^{\mathrm{eff}}_{\mathrm{EL2}} = 4 \times 10^{14}$ cm^{-3} is evaluated, which is in good agreement with data in Table I.

V. SUMMARY

SI GaAs, biased with dc voltages larger than a fixed critical voltage, shows oscillations in the current due to the presence of a high-field domain, which forms at the cathode, propagates in the bulk, and disappears at the anode. The formation of the domain is due to the negative differential resistance in the $j-E$ curve, which makes the homogeneous electric-field distribution unstable against random fluctuation in the space charge. Once the domain is formed, it propagates with constant velocity and preserves its shape. It is thus possible to apply the experimental solution to a set of equations that describes the system to obtain a microscopic description of the domain structure. In this way we clarify the complementary role played by electrons in the conduction band, which are depleted and are consequently responsible for the resistance of the domain and the electrons in the EL2 levels, which are the source of the space-charge dipole. Moreover, the trapping coefficient C_n has been evaluated, showing an electric-field enhancement of a factor of 10, which begins at a very low field ($\sim$0.4 kV/cm).

Increasing the applied voltages, the current oscillations are no longer periodic. This fact is related to the finite length of the sample, which does not allow a complete formation of the domain. The annihilation of one domain at the cathode then influences the formation of the next one at the anode and thus its final size. Therefore, there is a recursive iteration, which leads to chaotic oscillations in the current.

[1] V. A. Samuilov, in *Nonlinear Dynamics of Pattern Formation in Semiconductor and Devices*, edited by F.-J. Niedernostheide (Springer, Berlin, 1995), p. 220.
[2] E. Schöll, Physica B **135**, 271 (1985).
[3] J. Pozela, A. Namajunas, A. Tomasevicius, and J. Ulbikas, Appl. Phys. A **48**, 181 (1989).
[4] E. Schöll, *Nonequilibrium Phase Transitions in Semiconductors* (Springer-Verlag, Berlin, 1987).
[5] B. Willing and J. C. Maan, Phys. Rev. B **49**, 13 995 (1994).
[6] D. C. Northrop, P. R. Thornton, and K. E. Trezise, Solid State Electron. **7**, 17 (1964).
[7] H. K. Sacks and A. G. Milnes, Int. J. Electron. **28**, 565 (1970); **30**, 49 (1971).
[8] B. K. Ridley and P. H. Wisbey, Brit. J. Appl. Phys. **18**, 761 (1967); B. K. Ridley, J. J. Crisp, and F. Shishiyony, J. Phys. C **5**, 187 (1972); M. F. Leach and B. K. Ridley, *ibid.* **11**, 2265 (1987).

[9] D. A. Johnson *et al.*, Appl. Phys. Lett. **51**, 1152 (1987).
[10] G. N. Marakas *et al.*, Solid State Electron. **32**, 1887 (1989).
[11] U. Rau *et al.*, Phys. Lett. A **152**, 356 (1991).
[12] S. W. Teitsworth, R. M. Westervelt, and E. E. Haller, Phys. Rev. Lett. **51**, 825 (1983).
[13] M. Kikuchi, M. Suzuki, and T. Shibuya, Jpn. J. Appl. Phys. **1**, 188 (1962).
[14] D. G. Seiler, C. L. Littler, R. J. Justice, and P. W. Milonni, Phys. Lett. **108A**, 462 (1985).
[15] M. Kaminska, J. M. Parsey, J. Lagowski, and H. C. Gatos, Appl. Phys. Lett. **41**, 989 (1982).
[16] D. C. Look, Semicond. Semimet. **38**, 91 (1993).
[17] V. Ya. Prinz and B. A. Boblyev, Sov. Phys. Semicond. **14**, 1097 (1981).
[18] S. P. McAlister, Z.-M. Li, and D. J. Day, Can. J. Phys. **69**, 207 (1991).
[19] M. A. Abdela and B. K. Jones, Solid State Electron. **36**, 237 (1993).
[20] Y. V. Vorobev, E. I. Tolpygo, and M. K. Sheinkman, Phys. Status Solidi B **123**, 295 (1984).
[21] G. N. Marakas, W. Porod, D. A. Johnson, and D. C. Ferry, Physica B **134**, 276 (1985).
[22] J. Pozela, A. Tomasevicius, and J. Ulbikas, Solid State Electron. **31**, 805 (1988).
[23] J. Lusakowski, M. Jezewski, W. Knap, and W. Kuszko, Acta Phys. Pol. A **73**, 183 (1988).
[24] Z. S. Gribnikov, K. Hess, and G. A. Kosinovsky, Appl. Phys. Lett. **77**, 1337 (1995).
[25] S. M. Sze, in *Physics of Semiconductor Devices* (Wiley, Singapore, 1981).
[26] F. Piazza, P. C. M. Christianen, and J. C. Maan, Appl. Phys. Lett. **69**, 1909 (1996).
[27] S. Makram-Ebeid and M. Lannoo, Phys. Rev. B **25**, 6406 (1982).
[28] M. Rajbenbach, J. M. Verdiell, and J. P. Huijnard, Appl. Phys. Lett. **51**, 1152 (1987).
[29] D. A. Johnson, R. A. Puechner, and G. N. Marakas, J. Appl. Phys. **67**, 300 (1990).
[30] W. Knap *et al.*, Solid State Electron. **31**, 813 (1988).